# Journal of Materials Chemistry A

Accepted Manuscript


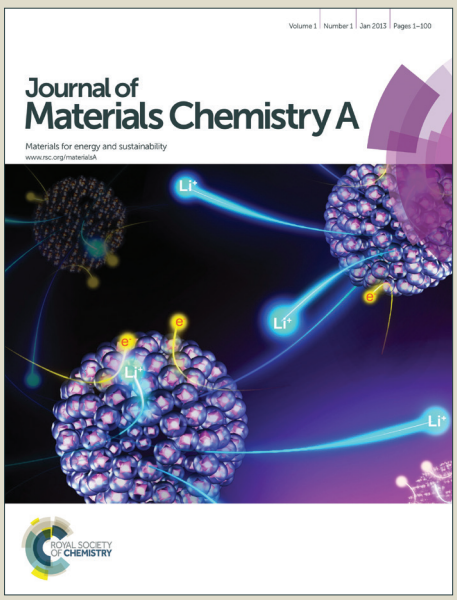





ROYAL SOCIETY OF CHEMISTRY

www.rsc.org/materialsA

# A table of contents entry

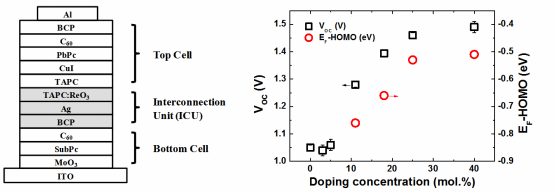


The electronic structure of an interconnection unit affects not only open circuit voltage but also fill factor in the tandem organic solar cells.

Journal Name

RSCPublishing

ARTICLE

# Correlation of the electronic structure of an interconnection unit with the device performance of tandem organic solar cells

Cite this: DOI: 10.1039/x0xx00000x

Received 00th January 2012,
Accepted 00th January 2012

DOI: 10.1039/x0xx00000x

www.rsc.org/

Hyun-Sub Shim[a], Jung-Hung Chang[b], Seung-Jun Yoo[a], Chih-I Wu[b] and Jang-Joo Kim[a,*]

We report the correlation of the electrical properties of the *p*-doped layer in an interconnection unit with the performance of tandem organic photovoltaic (TOPV) cells where the interconnection unit (ICU) is composed of electron-transporting layer (ETL)/metal/*p*-doped hole-transporting layer (*p*-HTL) by systematically varying the doping concentration of the *p*-HTL in the ICU. The open circuit voltage is significantly increased as the doping concentration of the *p*-HTL increases due to the reduction of the difference between the Fermi level and the highest occupied molecular orbital level of the *p*-HTL. The fill factor is also enhanced with increases in the doping concentration of the *p*-HTL due to the enhancement of the conductivity in the *p*-HTL and efficient hole transport at the interface between Ag and *p*-HTL through the tunneling process, rather than through the thermionic process.

## Introduction

Organic photovoltaic (OPV) cells have been shown to have lower efficiency than inorganic solar cells.[1,2] One of the reasons is the narrow absorption band of the organic materials used as active layers in OPVs. Tandem organic photovoltaic (TOPV) cells are a potential candidate to extend the absorption range of the solar spectrum in the devices.[3-8] TOPVs are composed of more than two subcells whose absorption overlap is minimized for the efficient use of solar photon flux and the interconnection unit (ICU), which should be transparent in the absorption range of subcells to reduce optical losses and ensure suitable energy level alignments between the subcells to minimize voltage losses. In addition, it would be desirable if they worked as optical spacers to match the current between the top and bottom cells.[8-11]

Various structures have been reported for the vacuum deposited ICUs, which can be classified into two systems: thin metal combined with metal oxide, or the *p*-doped layer and *p*-*n* junctions using *p*- and *n*-doped layers.[8, 11, 13-17] Both techniques show efficient charge recombination in the ICUs with minimized open circuit voltage ($V_{OC}$) loss. In terms of the optical spacer, however, metal oxide in the ICU does not work properly due to the decrease in the conductivity with increasing thickness of the metal oxide layer, resulting in the reduction of the fill factor (*FF*).[17] In contrast, the doped layer can be used as an optical spacer because it does not affect the device's performance electrically.[7-11] In other words, the generated carriers in the subcells can reach the recombination contact through the doped layers with few energetic barriers.

Electrical doping is widely used for efficient charge injection or extraction in organic electronics.[18-24] It is also in use for the charge generating units (CGUs) in tandem organic light emitting diodes.[23, 24] The mechanisms of charge generation by electrical doping in the CGUs are well established.[23, 24] For instance, the charge carrier generation layers in the CGUs consisting of *p*-doped hole-transporting layer (*p*-HTL)/1,4,5,8,9,11-hexaazatriphenylene hexacarbonitrile (HATCN)/*n*-doped electron-transporting layer (*n*-ETL) depends on the vacuum level shift at the HATCN/*n*-ETL and the free carrier density of the ETL rather than the lowest unoccupied molecular orbital (LUMO) level of the ETL.[23] In the TOPV cells, however, the operation mechanism of the doped layer in the ICUs has not been systematically investigated yet.

In this paper, we systematically investigated the effect of the electrical properties of the *p*-doped layer in the ICU composed of ETL/metal/*p*-HTL on the performance of a TOPV cell. $V_{OC}$ is enhanced as the doping concentration increases due to the reduction of the difference between the Fermi level and the highest occupied molecular orbital (HOMO) level of the *p*-HTL. *FF* is also enhanced as the doping concentration increases due to the lowering of the energetic barrier between the metal and the *p*-HTL for the hole transport and the increase of the conductivity in the *p*-HTL. Moreover, the depletion width is reduced as the doping concentration increases due to the increased carrier density in the doped layer, facilitating the tunneling process at the interface.

## Experimental

### Device fabrication

The 150 nm-thick ITO coated glass substrate was cleaned with acetone and isopropyl alcohol, and exposed to UV-$O_3$ for 10

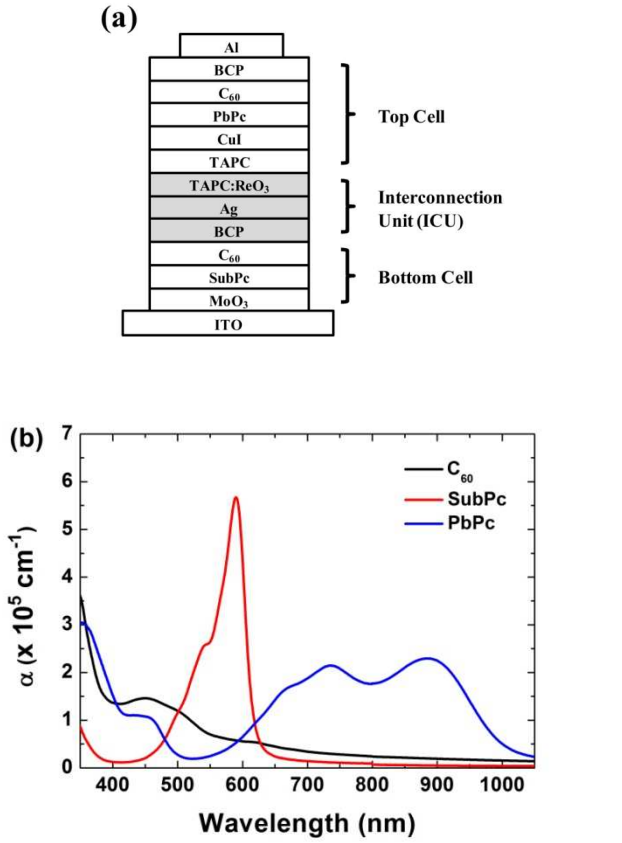


Figure 1. (a) The device structure of a tandem organic photovoltaic cell is composed of a bottom cell, top cell and an interconnection unit. (b) The absorption coefficient of organic materials used as donors and acceptors in the TOPV cell, which were deposited on glass.

min. before use. All the materials were thermally evaporated at a base pressure of < $10^{-7}$ Torr without breaking the vacuum. The *p*-doped layer in the ICU was formed using the co-evaporation of the 1,1-bis-(4-bis(4-methyl-phenyl)-amino-phenyl)-cyclohexane (TAPC) and rhenium oxide ($ReO_3$). The evaporation rate was varied from 0.01 Å/s to 0.25 Å/s for $ReO_3$ with a fixed rate of 1 Å/s for TAPC. The active area of each device was 4 $mm^2$ and more than four devices were fabricated to average the cell performance. After evaporation, the devices were encapsulated using an epoxy resin with glass cans in an $N_2$ environment.

### Device characterization

The UV-vis absorption spectra of the films were recorded with a VARIAN Cary 5000 UV-vis spectrophotometer. The current density-voltage (*J-V*) characteristics were measured under AM 1.5G solar simulator illumination (Newport, 91160A), and recorded using a Keithley 237 source measurement unit. The light intensity was calibrated using a standard Si-solar cell (NREL).

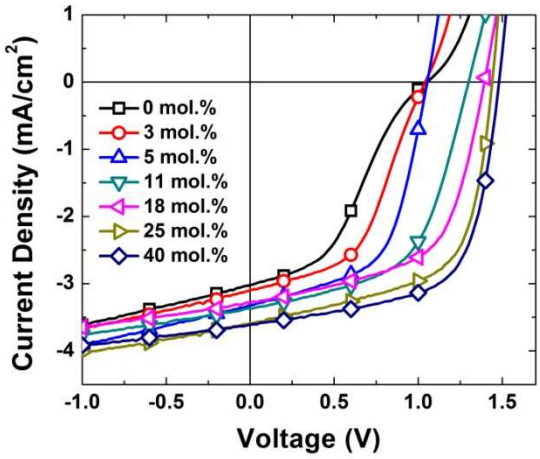


Figure 2. The *J-V* characteristics of tandem organic photovoltaic cells with varying the doping concentrations of the *p*-HTL in the interconnection unit under AM 1.5G illumination.

The ultraviolet photoemission spectra (UPS) were carried out in a three interconnected ultrahigh vacuum chamber. Organic materials and metal were evaporated on ITO in the separated evaporation chambers and were transferred to the analysis chamber. The UPS signals were measured using He Iα (21.2 eV) as the excitation source under a base pressure of $10^{-10}$ Torr. The kinetic energies of photoelectrons emitted from the sample were recorded by a hemispherical analyzer with an overall resolution of 0.05 eV.

## Results and discussion

Fig. 1a shows the device structure of the TOPV cell. The bottom cell is composed of 10 nm boron subphthalocyanine chloride (SubPc)/15 nm $C_{60}$ and the top cell is composed of 3 nm 1,1-bis-(4-bis(4-methyl-phenyl)-amino-phenyl)-cyclohexane (TAPC)/15 nm lead phthalocyanine (PbPc)/10 nm $C_{60}$. A 3 nm thick molybdenum oxide ($MoO_3$) layer was inserted between the ITO and SubPc layer to secure good hole injection through the junction. A 1 nm thick copper iodide (CuI) layer was deposited on the TAPC layer of the top cell to increase the absorption of the PbPc layer in the near-infrared region.[25, 26] The subcells are connected by the ICU, consisting of 3 nm bathocuproine (BCP)/0.3 nm Ag/8 nm rhenium oxide ($ReO_3$) doped TAPC where the BCP, Ag and $ReO_3$ doped TAPC layers are used as the ETL, recombination layer and the *p*-HTL, respectively. The doping concentration of the *p*-HTL is systematically varied from 0 to 40 mol.% in order to investigate the effect of the doping concentration on the TOPV cell. The absorption overlap between the donors in the top and bottom cell is minimized, as shown in Fig. 1b. The absorption of PbPc is extended into the near-infrared region because the copper iodide (CuI) inserted between TAPC and PbPc leads the PbPc molecules to form a more crystalline structure with a preferred orientation.[25, 26] The transmittance of the ICU is over 90%, fulfilling the requirement for optical transparency of the ICU.[5] In this study, the thicknesses of the layers in the TOPV cell are fixed and only the doping concentration of the *p*-HTL was systematically varied to exclude any optical effect on the performance of the TOPV cells.



 

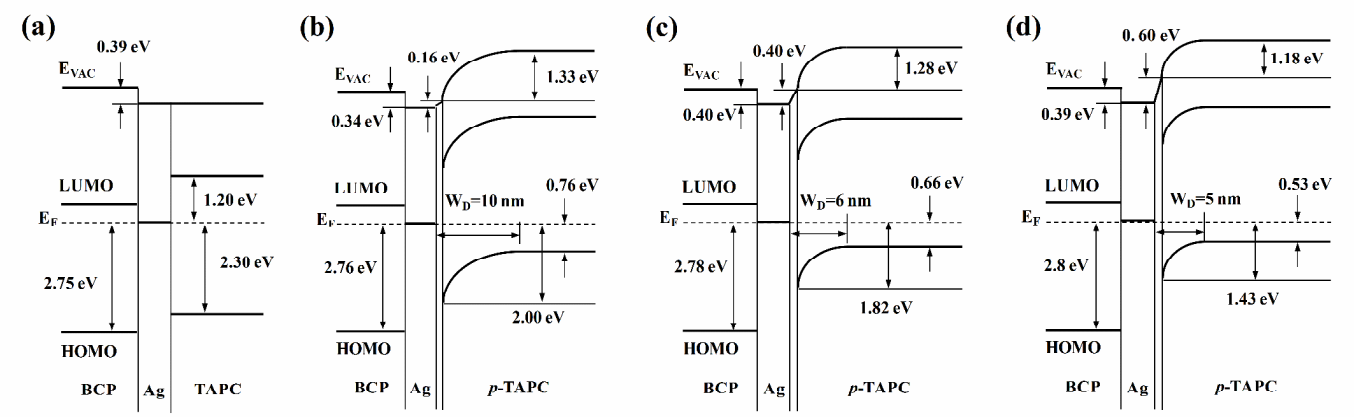


Figure 3. The schematic energy level alignment of BCP(3 nm)/Ag(0.3 nm)/*p*-TAPC with different doping concentrations of (a) 0 mol.%, (b) 11 mol.%, (c) 18 mol.% and (d) 25 mol.%.

Fig. 2 displays the photo-current density-voltage (*J-V*) characteristics with different doping concentrations measured under AM 1.5G solar illumination. Interestingly enough, the solar cell performances are significantly affected by the doping concentration of the *p*-HTL in the ICU. In this system, the theoretically simulated short circuit current density ($J_{SC}$) is 4.19 mA/cm$^2$, which was determined by using the transfer matrix method coupled with the exciton diffusion equation.[8] When an undoped layer is used in the ICU, an S-curve is generated with a $J_{SC}$ value of 3 mA/cm$^2$, $V_{OC}$ of 1.05 V, *FF* of 0.38 and a power conversion efficiency (*PCE*) of 1.19%, due to the resistance to the transportation of holes from the top cell to the recombination contact.[8, 20] The cell performance gradually improves as the doping concentation increases in the *p*-HTL up to a $J_{SC}$ value of 3.57 mA/cm$^2$, $V_{OC}$ of 1.49 V, *FF* of 0.64 and a *PCE* of 3.38%, when the 40 mol.% $ReO_3$ doped TAPC layer is used in the ICU. The doping concentration dependent performance of the TOPV cells are summarized in Table 1. The performances of the optimized single devices for the top and bottom cell are a $J_{SC}$ value of 4.11 mA/cm$^2$, $V_{OC}$ of 1.06 V, *FF* of 0.66 and *PCE* of 2.87% for the bottom cell, and a $J_{SC}$ value of 7.25 mA/cm$^2$, $V_{OC}$ of 0.46 V, *FF* of 0.61 and *PCE* of 2.03% for the top cell. The $V_{OC}$ loss in the TOPV cell is less than 2% compared to the sum of the top and bottom cell, indicating that the energy levels between the top and bottom cell are well aligned, which is the one of the main requirements of the ICU.

To understand the dependence of the $V_{OC}$ on the doping concentration of the *p*-HTL, ultraviolet photoelectron spectroscopy (UPS) measurements were performed using the He I (21.2 eV) as an excitation source under an ultra high vacuum of $10^{-10}$ torr. Fig. 3a-d displays the energy level alignment at thermal equilibrium for different doping concentrations. The vacuum level and the HOMO levels of each layer were obtained from the UPS spectra (Fig. S1) and the LUMO levels were determined using the reported band-gap.[27] The vacuum level shift between BCP and Ag is in the range of 0.34 eV~0.4 eV, and the Fermi level ($E_F$)–HOMO level of BCP is around 2.78 eV for all the doping concentrations. There is no vacuum level shift at the Ag/TAPC when the neat TAPC layer is used, as shown in Fig. 3a. As the doping level increases, the Fermi level in the *p*-HTL becomes closer to the HOMO level of the TAPC, as expected. This shift in the Fermi level must be related to the $V_{OC}$ of the TOPV cell as manifested in Fig. 4 where the variation of $V_{OC}$ and the $E_F$-HOMO level are plotted on the same scale against the doping concentration. Even though it is difficult to directly correlate the change in $V_{OC}$ with the $E_F$-HOMO level of the *p*-TAPC layer because of the possibility of a vacuum level shift at the interface between the *p*-TAPC and the intrinsic TAPC layer, the increase in $V_{OC}$ with the doping concentration can be interpreted based on the Fermi level shift of the *p*-HTL in the ICU. When the *p*-HTL is deposited on the Ag layer, a depletion layer is formed at the Ag/*p*-HTL and the depletion width becomes narrower as the doping concentration increases. It is interesting to note that there is a vaccum level shift at the Ag/*p*-HTL and its amount increases from 0.16 eV at the doping concentration of 11 mol.% to 0.6 eV at 25 mol.% doping, resulting in a reduced built-in potential at the *p*-HTL with increasing doping concentration, from 1.33 eV at a doping concentration of 11 mol.% to 1.18 eV at 25 mol.% doping, as shown in Fig. 3b-d. Therefore, the $E_F$-HOMO level of the *p*-HTL is reduced from 0.76 eV to 0.53 eV as the doping concentration increases from 11 mol.% to 25 mol.%., indicating that the energy level between the bottom cell and the top cell is

Table 1. Summary of solar cell performances with different doping concentrations of the *p*-HTL in the interconnection unit. The series resistance ($R_S$) is obtained by fitting the dark *J-V* curve with the Shockley diode equation.

| | PCE (%) | $J_{SC}$ (mA/cm$^2$) | $V_{OC}$ (V) | FF | Rs (Ωcm$^2$) |
|---|---|---|---|---|---|
| 0 mol.% | 1.19 ± 0.04 | 3.00 ± 0.03 | 1.05 ± 0.01 | 0.38 ± 0.01 | 30.34 ± 1.15 |
| 5 mol.% | 1.95 ± 0.05 | 3.29 ± 0.04 | 1.06 ± 0.02 | 0.56 ± 0.02 | 9.81 ± 0.23 |
| 11 mol.% | 2.41 ± 0.01 | 3.36 ± 0.01 | 1.28 ± 0.01 | 0.56 ± 0.02 | 8.32 ± 0.23 |
| 18 mol.% | 2.62 ± 0.03 | 3.23 ± 0.03 | 1.39 ± 0.01 | 0.58 ± 0.01 | 6.76 ± 0.25 |
| 25 mol.% | 3.15 ± 0.03 | 3.57 ± 0.03 | 1.46 ± 0.01 | 0.61 ± 0.01 | 4.47 ± 0.08 |
| 40 mol.% | 3.38 ± 0.02 | 3.57 ± 0.03 | 1.49 ± 0.02 | 0.64 ± 0.01 | 4.96 ± 0.07 |

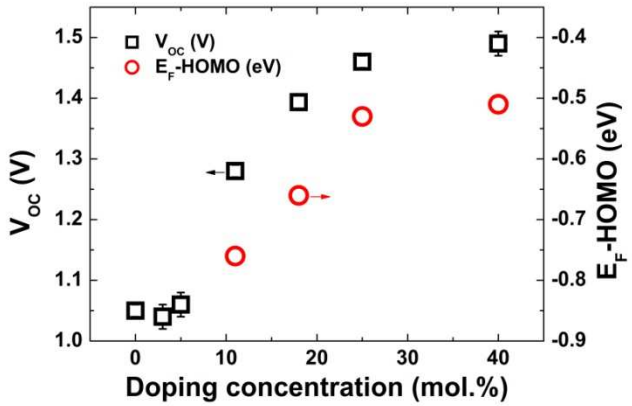


Figure 4. The $V_{OC}$ dependence (left side) and the difference between the Fermi level ($E_F$) and the HOMO level of the *p*-HTL (right side) as a function of the doping concentration of *p*-HTL.

better aligned with reduced the voltage loss in the ICU.

Another important parameter is the depletion width ($W_D$), which is expressed as follows

$$W_D = \sqrt{\frac{2\varepsilon_0\varepsilon_r V_{bi}}{qp}} \quad (1)$$

where $p$ is the free hole density in the *p*-HTL, $V_{bi}$ is the built-in potential and $\varepsilon_0$ and $\varepsilon_r$ are the absolute and relative dielectric constants, respectively. $W_D$ is inversely proportional to the free hole density in the *p*-HTL. Therefore, it becomes narrower as the doping concentration increases due to the increase of the free hole density in the *p*-HTL. $W_D$ is 10 nm in the 11 mol.% $ReO_3$ doped TAPC layer, which is longer than its thickness of 8 nm in the TOPV cell. Therefore, the HOMO level is not fully shifted, resulting in an increase in the $E_F$-HOMO level of the *p*-HTL from 0.76 eV to 0.84 eV. This fact indicates that the the thickness of the doped layer in the ICU should be thicker than its depletion width to minimize the $V_{OC}$ loss.

In order to investigate the relationship between the doping concentration of the *p*-HTL in the ICU and the *FF* of the TOPV cells, the series resistance ($R_S$) is obtained by fitting the dark *J-V* curve with the Shockley diode equation, as shown in Fig. 5a. The *FF* value is enhanced up to 0.64 from 0.38 as the doping concentration increases from 0 to 40 mol.% in the *p*-HTL, which is inversely proportional to the $R_S$ value. In this study, the doping concentration of the *p*-HTL is only changed with a fixed thickness of all the layers in the TOPV cell. Therefore, the change in the $R_S$ value is directly related to the change in the conductivity in the *p*-HTL and the interface properties between the recombination contact and the top cell. The conductivity of the *p*-HTL is obtained by using $Mp^{++}p^{+}p^{++}M$ structures of ITO/TAPC: 50 mol.% $ReO_3$ (10 nm)/ TAPC: X mol.% $ReO_3$ (100 nm) [X = 0, 5, 11, 18, 25, 40]/ TAPC: 50 mol.% $ReO_3$ (10 nm)/Al (100 nm), as shown in Fig. 5b (See Fig. S2a,b for the original data).[28] The conductivity is enhanced from $1.43 \times 10^{-8}$ S/cm to $5.19 \times 10^{-7}$ S/cm as the doping concentration increases from 5 mol.% to 40 mol.%, respectively, which is at least two orders of magnitude greater than that of the intrinsic TAPC layer (~ $10^{-10}$ S/cm). This fact

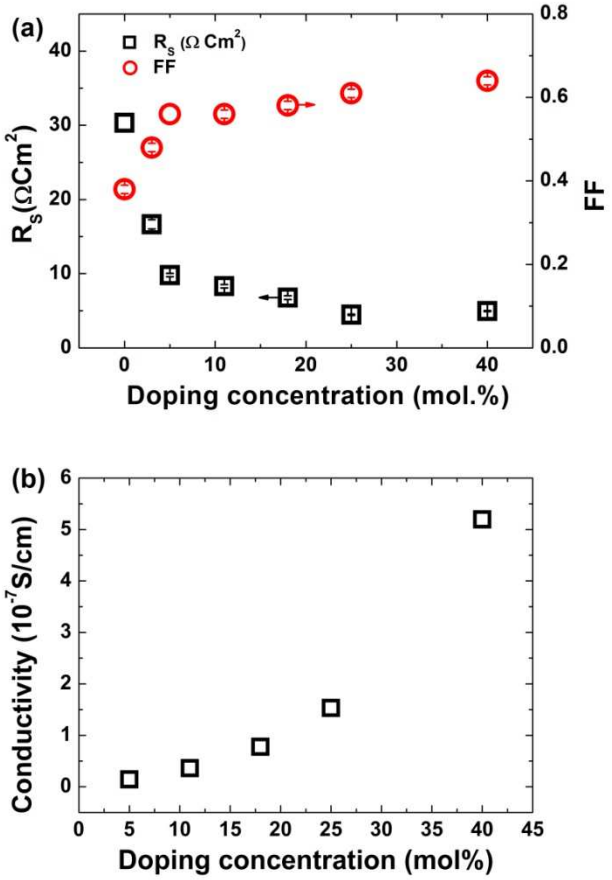


Figure 5. (a) The dependence of the series resistance (left side) and fill factor (right side) as a function of the doping concentration of the *p*-HTL. (b) The conductivity of the *p*-HTL as a function of the doping concentration, obtained from the current density-electric field (*J-F*) characteristics.[28]

indicates that holes can be transported efficiently to the recombination contact through the bulk of the *p*-HTL with an increasing doping concentration of *p*-HTL.

The interface property between Ag and the *p*-HTL is also an important factor affecting the *FF* in the TOPV cells. When neat TAPC is used in the ICU, the energetic barrier for holes to overcome for transport at the Ag/TAPC interface is 2.3 eV. This indicates that holes cannot be injected from Ag to the TAPC layer and be accumulated at Ag/TAPC, resulting in an S-curve with a reduced *FF*.[20, 29] When the *p*-HTL is used in the ICU, the energetic barrier, shown in Fig. 3a-d, which is estimated for a *p*-HTL thickness of 0.8 nm in the UPS data, is reduced from 2 eV to 1.43 eV as the doping concentration increases from 5 mol.% to 25 mol.%, as shown in Fig. 3a-d. However, this barrier is too large for holes to overcome for transport at the interface. In this system, $W_D$ is reduced from 10 nm at the doping concentration of 5 mol.% to 5 nm at 25 mol.% doping as shown in Fig. 3a-d. This fact represents that the possibility of the tunneling process is enhanced as the doping concentration increases. Therefore, holes can be transported more efficiently at the Ag/*p*-HTL interface through the tunneling process rather than the thermionic process as the doping concentration of the *p*-HTL increases, resulting in an enhanced *FF*.

## Conclusion

In conclusion, we have demonstrated a correlation between the electrical properties of the *p*-HTL in the ICU and the device performance of TOPV cells by systematically varying the doping concentration of the *p*-HTL. The $V_{OC}$ value in the TOPV cells increases with increases in the doping concentration due to the reduction of the difference between the Fermi level and the HOMO level of the *p*-HTL. The *FF* is also enhanced with increases in the doping concentration, due to the enhancement of the conductivity in the p-HTL and efficient hole transport at the interface between Ag and the *p*-HTL through the tunneling process rather than the thermionic process.

## Acknowledgements

This work was supported by the New & Renewable Energy Technology Development Program of the Korea Institute of Energy Technology Evaluation and Planning (KETEP) grant funded by the Korea government Ministry of Knowledge Economy (No. 20113020010070) and under the framework of the international cooperation program managed by the National Research Foundation of Korea (2012K2A1A2033115)

### Notes and references

[a] Department of Materials Science and Engineering and the Center for Organic Light Emitting Diode, Seoul National University, Seoul 151-74, South Korea. Fax: 82 889 8702; Tel: 82 2 880 7893; E-mail: jjkim@snu.ac.kr
[b] Department of Electrical Engineering and Graduate Institute of Photonics and Optoelectronics, National Taiwan University, Taipei, Taiwan 10617, ROC

†Electronic Supplementary Information (ESI) available: the raw data of UPS measurement and *J-V* characteristics of hole- and electron-only device . See DOI: 10.1039/b000000x/

1 M. Riede, T. Mueller, W. Tress, R. Schueppel. K. Leo, *Nanotechnology*, 2008, 19, 424001.
2 M. He, F. Qiu, Z. Lin, *J. Phys. Chem. Lett*. 2013, 4, 1796.
3 T. Ameri, N. Li, C. J. Brabec, *Energy Environ. Sci*. 2013, 6, 2390.
4 J. You, L. Dou, K. Yoshimura, T. Kato, K. Ohya, T. Moriarty, K. Emery, C. C. Chen, J. Gao, G. Li, Y. Yang, *Nat. commun*. 2013, 4, 1446.
5 W. Li, A. Furlan, K. H. Hendriks, M. M. Wienk, R. A. Janssen, *J. Am. Chem. Soc*. 2013, 135, 5529.
6 B. E. Lassiter, J. D. Zimmerman, A. Panda, X. Xiao, S. R. Forrest, *Appl. Phys. Lett*. 2012, 101, 063303.
7 M. Riede, C. Uhrich, J. Widmer, R. Timmreck, D. Wynands, G. Schwartz, W.-M. Gnehr, D. Hildebrandt, A. Weiss, J. Hwang, S. Sundarraj, P. Erk, M. Pfeiffer, K. Leo, *Adv. Funct. Mater*. 2011, 21, 3019.
8 H.-S. Shim, S.-Y. Kim, J. W. Kim, T.-M. Kim, C.-H. Lee, J.-J. Kim, *Appl. Phys. Lett*. 2013, 102, 203903.
9 J. Yang, R. Zhu, Z. Hong, Y. He, A. Kumar, Y. Li, Y. Yang, *Adv. Mater*. 2011, 23, 3465.
10 R. Schueppel, R. Timmreck, N. Allinger, T. Mueller, M. Furno, C. Uhrich, K. Leo, M. Riede, *J. Appl. Phys*. 2010, 107, 044503.
11 E. New, T. Howells, P. Sullivan, T. S. Jones, *Org. Electron*. 2013, 14, 2353.
12 D. Cheyns, B. P. Rand, P. Heremans, *Appl. Phys. Lett.* 2010, 97, 033301.
13 R. Timmreck, S. Olthof, K. Leo, M. K. Riede, *J. Appl. Phys.* 2010, 108, 033108.
14 M. Zhang, H. Wang, C. W. Tang, *Org. Electron.* 2012, 13, 249.
15 J. Yang, W. Chen, B. Yu, H. Wang, D. Yan, *Org. Electron.* 2012, 13, 1018.
16 J. Li, Q.-Y. Bao, H.-X. Wei, Z.-Q. Xu, J.-P. Yang, Y.-Q. Li, S.-T. Lee, J.-X. Tang, *J. Mater. Chem.* 2012, 22, 6285.
17 J. A. Macko, R. R. Lunt, T. P. Osedach, P. R. Brown, M. C. Barr, K. K. Gleason, V. Bulovic, *Phys. Chem. Chem. Phys.* 2012, 14, 14548.
18 D.-S. Leem, J.-H. Lee, J.-J. Kim, J.-W. Kang, *Appl. Phys. Lett.* 2008, 93, 103304.
19 B. Lüssem, M. Riede, K. Leo, *Phys. status solidi A* 2013, 210, 9.
20 D.-H. Kim, T.-M. Kim, W.-I. Jeong, J.-J. Kim, *Appl. Phys. Lett.* 2012, 101, 153303.
21 J.-H. Lee, J.-J. Kim, *Phys. status solidi A* 2012, 209, 1399.
22 J.-H. Lee, D.-S. Leem, H.-J. Kim, J.-J. Kim, *Appl. Phys. Lett.* 2009, 94, 123306.
23 S. Lee, J.-H. Lee, J.-H. Lee, J.-J. Kim, *Adv. Funct. Mater.* 2012, 22, 855.
24 M. Kröger, S. Hamwi, J. Meyer, T. Dobbertin, T. Riedl, W. Kowalsky, H.-H. Johannes, *Phys. Rev. B* 2007, 75, 235321.
25 H.-S. Shim, H. J. Kim, J. W. Kim, S.-Y. Kim, W.-I. Jeong, T.-M. Kim, J.-J. Kim, *J. Mater. Chem.* 2012, 22, 9077.
26 H. J. Kim, H.-S. Shim, J. W. Kim, H. H. Lee, J.-J. Kim, *Appl. Phys. Lett.* 2012, 100, 263303.
27 V. I. Adamovich, S. R. Cordero, P. I. Djurovich, A. Tamayo, M. E. Thompson, B. W. D'Andrade, S. R. Forrest, *Org. Electron*. 2003, 4, 77.
28 S.-J. Yoo, J.-H. Lee, J.-H. Lee, J.-J. Kim, *Appl. Phys. Lett.* 2013, 102, 183301.
29 W. Tress, K. Leo, M. Riede, *Adv. Funct. Mater.* 2011, 21, 2140.